The Vogel−Fulcher−Tamman Equation Investigated by Atomistic Simulation with Regard to the Adam−Gibbs Model

Noureddine Metatla and Armand Soldera*

Département de Chimie, Université de Sherbrooke, Sherbrooke, Québec J1K 2R1, Canada

Received August 8, 2007; Revised Manuscript Received October 20, 2007

ABSTRACT: Many efforts in experimental and theory are dedicated to study the puzzling problem of glass transition. With the involvement of molecular modeling, a fresh look at this intricate phenomenon was taken. Nevertheless, the difficulty to accurately probe all the domains of times necessary to describe this process still remains. Moreover, using a full-atomic description to account for equilibrated systems has been called into question. However, such depiction offers a special regard since it could deal with small modifications in the polymer architecture. From an appropriate selection of phase space, it was shown that atomistic simulation was able to link simulated and experimental glass transition temperatures of vinylic polymers using the established Williams−Landel−Ferry equation. Consequently, atomic insight into the glass transition phenomenon can be gained from a comparison of simulated data with actual models and experimental data. In this paper, the different parameters intervening in the Vogel−Fulcher−Tamman equation stemming from the local dynamics of a series of vinylic polymers are thus compared. Their behavior yields an atomistic viewpoint of the Adam−Gibbs model.

1. Introduction

The glass transition remains a perplexing problem, although great experimental, theoretical, and simulation efforts have been made toward a better understanding. Numerous problems remain unsolved: the crossover region, multiple relaxations, cooperative processes, etc.[1,2] Additionally, the huge domain of length and time scales covered by this phenomenon implicitly yields numerous theories and models. Those currently employed are the free volume theory,[3] the Adam−Gibbs (AG) theory,[4,5] the coupling mode theory (CMT),[6] the coupling model (CM),[7,8] the energy landscape model,[9−11] and the spatially heterogeneous dynamics.[12,13] Their domain of applicability and their strength in accurately depicting the glass transition are still sources of debate. The lack of consensus stems greatly from the fact that no experimental technique supports one specific theory.[6,14−17]

Regarding the treatment of this sensitive problem, molecular modeling became an essential asset since it links theory and experiment. Different kinds of molecular simulations are used to deal with all the ranges of length and time scales in order to describe the behavior of the glass-forming liquids and thus to connect together the glass transition theories: molecular dynamics (MD),[18,19] coarse-grained simulations,[20] and Monte Carlo simulations.[21,22] Because of the small domains of time covered by the all-atom approach, atomistic simulation (AS) was not considered suitable to deal with the glass transition phenomenon.[23] However, simulated glass transition temperatures (T_gs) of a series of vinylic polymers have been shown to be correlated to experimental T_gs through the Williams−Landel−Ferry (WLF) equation.[24] Valuable information at the atomistic level can be extracted from those simulations if the correlations associated with the computed property do not exceed the size of the simulated system. Resulting conclusions can then be employed in addition to experiments, coarse-grained simulation data, and theories to give a better description of the glass transition phenomenon.

Since AS adequately mimics the glass transition of polymers, it can be worthwhile to evaluate the different models from an atomistic viewpoint. Among the theories, the AG model offers a particular perspective on the study of the glass transition of polymers since it gives the theoretical basis of the widely used Vogel−Fulcher−Tamman (VFT) equation. As reported by Cangialosi et al.,[25] it is generally accepted that this equation gives a good description of the relaxation time with the temperature. It actually relates the correlation time to an effective activation energy and a vanishing mobility temperature, T_0, also referred to as the Vogel temperature.[26] In fact, as the polymeric system cools down, the available number of configurations decreases, resulting in an increase of the correlation length and a non-Arrhenius behavior of the relaxation time.[27] The Arrhenius behavior occurs at high temperature when the activation energy is the same for all the segments, i.e., when the length of a bead, or a cooperatively rearranging region (CRR), is reduced to unity. This CRR corresponds to an average number of repeat units that relax together independently of their environment. The AG equation thus relates thermodynamics (entropy) and dynamics (activation energy).[27]

The concept of growing CRR as the temperature is lowered and the existence of an energy barrier are two strong arguments that make the AG model particularly useful in describing the glass transition. The purpose of this text is to explore the possibilities offered by AS to provide atomistic details on parameters intervening in the VFT equation with regard to the AG model, in the case of vinylic polymers.[27]

The studied polymers were chosen according to the relative rigidity of their side chain and the impact of the stereoregularity along their chain to the T_g value. Moreover, they are representative of the three groups introduced by Dubowicz et al. in order to classify polymers according to their architecture and their T_g:[28,29] flexible−flexible (FF), flexible−stiff (FS), and stiff−flexible (SF). In the FF group, there is the polyethylene (PE). Polystyrene (PS) and isotactic and syndiotactic poly(α-methylstyrene) (i-PαMS and s-PαMS) go into FS group. Poly(methyl acrylate) (PMA) and isotactic and syndiotatic poly(methyl methacrylate) (i-PMMA and s-PMMA) make up the SF group. Except for PE, they all possess a side chain: an ester group for PMA and PMMA and a phenyl group for PS and PαMS. The presence of an additional α-methyl group in PMMA and PαMS

* Corresponding author: e-mail Armand.Soldera@USherbrooke.ca; Ph +1-819-821-7650; Fax +1-819-821-8017.

10.1021/ma071788+ CCC: $37.00
Published on Web 12/04/2007

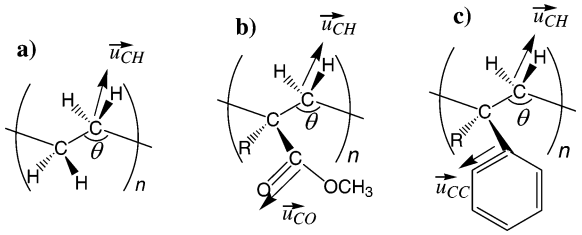

Figure 1. Repeat units of the studied vinylic polymers with vectors used to uncovered local dynamics: $\vec{u}_{CH}$, $\vec{u}_{CO}$, and $\vec{u}_{CC}$. (a) PE; (b) PMA (R = H) and PMMA (R = CH_3); (c) PS (R = H) and PαMS (R = CH_3).

imparts to these polymers different T_gs according to the tacticity of their chain,[30] while no significant difference in T_gs is observed between stereomers of PMA and PS. Their scheme is displayed in Figure 1. AS is particularly well suited to treat these polymers since they differ from each other by small variations in atomic interaction combinations but give rise to important changes in the values of T_gs, from −80 to 200 °C.

2. Procedure

All the details to get the final structure are exposed in a previous publication.[31] The selection of configurations upon which calculations are performed is based on a specific method using the self-avoiding walk procedure to generate configurations,[32] a comparison with experimental data to select the apposite region of the configurational space, a simulated annealing procedure to relax the system, and finally a uniform hydrostatic compression to get the initial configurations. From these configurations, the dilatometric technique is carried out to determine the T_g.[33] As the system cools down, the specific volume, i.e., the inverse of density, is reported for different temperatures. The departure from a linear relationship between the specific volume and the temperature yields the value of the T_g. To apply this procedure to polymeric systems, optimized configurations are gently heated to 800 K. Thereafter, the system is cooled down to 240 K by 20 K steps. Configurations are then kept at each temperature in the NPT ensemble (i.e., constant number of particles, pressure, and temperature) for 100 ps, 500 ps, or 1 ns. How long the system remains at one temperature determines the cooling rate.[34] Three cooling rates, q, are used: $q_1 = 1.2 \times 10^{13}$ (20 K/100 ps), $q_2 = 2.4 \times 10^{12}$ (20 K/500 ps), $q_3 = 1.2 \times 10^{12}$ K/min (20 K/1000 ps).

All the MD simulations are carried out using the first-generation OPLS force field with the DL_POLY code.[35,36] The equations of motion are integrated using the Verlet-leapfrog integration algorithm with a 1 fs integration time step.[37] During the MD simulations, the Berendsen thermostat and barostat are used in order to keep the system at the chosen temperature and pressure.[38] The nonbonded interactions are computed using the Ewald summation; a nonbond cutoff of 10 Å is selected.[39] For each configuration, above the T_g, an additional MD simulation of 1 ns duration in the NPT ensemble is applied. From these simulations, configurations were saved every 0.5 ps. These trajectories were used to perform analysis of the local dynamics.[40,41]

To study an appropriate dynamics, one bond, $\vec{u}$, is selected. The rotational autocorrelation function (RACF) associated with this bond is then computed from a MD trajectory. It allows the computation of the second Legendre polynomial term, $P_2(t)$:

$$P_2(t) = \frac{3\langle(\vec{u}(t)\cdot\vec{u}(0))^2\rangle - 1}{2} \tag{1}$$

The correlation time is computed from the integral of $P_2(t)$ over all the time. Since that cannot be done practically, a stretched exponential, or Kolsraush−Williams−Watt (KWW) function, $\exp[-(t/\tau)^{\beta_{KWW}}]$, is employed to fit $P_2(t)$.[42] Because of the reduced number of data at large times in the computation of the RACF, only the first 800 ps on a 1 ns duration is used.[43] Moreover, this fit is not applied at very low times where librational motions occur.[40] Since only motions of larger magnitude are of interest in this study, the KWW function is of practical use for this fit.

The correlation time is thus computed at different temperatures above T_g for the 10 selected configurations of each of the nine polymers, a number which includes the stereoregular polymers. To relate the different correlation times with the different temperatures, two equations can be employed: WLF (eq 2) and VFT (eq 3). Since the AG model is the theoretical foundation of VFT, this latter equation is specifically employed to fit the correlation times at different temperatures. However, some parameters extracted from the WLF equation are used to help in interpreting the simulation data. In fact, the two equations are equivalent in the time domain of the AS.[23,44]

$$\log\left[\frac{\tau_c(T)}{\tau_c(T_g)}\right] = -\frac{C_1^g(T - T_g)}{C_2^g + T - T_g} \tag{2}$$

$$\tau_c(T) = \tau_{VFT}\exp\left(\frac{B}{T - T_0}\right) \tag{3}$$

where τ_{VFT}, B, T_0, C_1^g, and C_2^g are fitted parameters. The equivalence between the two equations involves the following equalities: $B = \ln(10)C_1^gC_2^g$ and $C_2^g = T_g - T_0$.

Study of the correlation time, and thus the determination of B and T_0 in eq 3, unveils the dynamics associated with a specific segment of the polymer chain. The selection of the segment is thus of great importance. Two bonds are chosen, and their location inside the repeat unit is displayed in Figure 1. The bond vector $\vec{u}_{CH}$ reveals the backbone motion, while bond vectors $\vec{u}_{CO}$ and $\vec{u}_{CC}$ uncover the backbone and side-chain motions simultaneously for the PMA and PMMA and for PS and PαMS, respectively.[40] Some attempts have been made to separate the two motions from the $P_2(t)$ graph without success. Accordingly, the dynamics resulting from such coupling inside the polymer chain can be studied. Finally, it has to be pointed out that since the differences in T_g values between iso- and syndiotactic configurations of PMA and PS are smaller than the margin of error, the reported data correspond to the average of both configurations.

3. Results and Analysis

3.1. Overview of the AG Theory. At high temperature, in the Debye relaxation regime, bonds freely rotate. At a specific point, as the temperature is lowered, motions are collective and the AG theory becomes effective.[27] According to this model, participation of larger grouping of segment, thus defining a CRR where segment motion is collective, is progressively growing as the glass transition is approached. It becomes infinitely long at T_0 where no motions occur, except vibrations. This increasing cooperativity is envisioned as a loss of the configurational entropy, S_{conf}. The correlation time is thus expressed as follows:

$$\tau_c(T) = \tau_{VFT}\exp\left(\frac{C}{TS_{conf}}\right) \tag{4}$$

where C is a constant. The central assumption in the AG theory

is that $S_{conf} \sim \Delta s$, i.e., the difference in the entropy between the liquid and the glass phases. The entropy stemming from the residual vibrations is thus neglected. Considering the variation of the heat capacity between the two phases as hyperbolic dependent on temperature with K, the constant of proportionality, the correlation time reduces to

$$\tau_c(T) = \tau_{VFT} \exp\left(\frac{DT_0}{T - T_0}\right) \quad (5)$$

D is called the fragility index, or the strength index[45] since it describes the strength of temperature dependence of relaxation time,[46] and is equal to the ratio C/K. Comparing this equation to the VFT equation (eq 3) yields the following equality: $DT_0 = B$. A particular expression for D has been derived by Angell,[27] where differentiation between the kinetic (numerator) and thermodynamic (denominator) parts was established:

$$D = \frac{\delta\mu s_c^* k_b^{-1}}{K} \quad (6)$$

$\delta\mu$ is the chemical potential difference between liquid and glass states; it plays the role of a free energy barrier to the cooperative rearrangement. k_b is the Boltzmann constant. s_c^* corresponds to the minimum of entropy; a value of $k_b \ln 2$ is usually considered, but $k_b \ln 2^3$ has been preferred by Hodge.[47]

The purpose of this article is to use simulation at the atomistic level to correlate the VFT and AG parameters to polymer characteristics. A global analysis of the different terms intervening in the fragility index could not be performed at this point since $\delta\mu$ depends on the molecular weight. Specific comparison between two polymer configurations, as in the case of PMMA, could be carried out and will be presented in a dedicated paper. The discussion in this article is specifically centered on a comparative study of T_0, B, and D for the two studied dynamics and the different polymers. T_0 and B directly stem from the fit of the correlation time by the VFT equation. The fragility index D, which comes from the AG equation, is deduced from those parameters. A correlation between AS results and AG model can thus be established. Behavior of these three parameters with T_g is considered using data obtained by MD simulation performed at the lowest cooling rate, q_3. The specific impact of the cooling rate on these parameters is exposed in the final part.

3.2. Behavior of the Vogel Temperature, T_0. According to the AG model, the vanishing temperature, or Vogel temperature, T_0, could be equated to T_g during an infinitely slow process where the glass transition would become a true second-order transition.[48] It has to be pointed out that there are different opinions in the literature whether it is equivalent to the Kauzman temperature.[46] However, since configurational and thermodynamic entropies have been equated, no difference between the two temperatures is considered. The Vogel temperature is primarily regarded as a fitting parameter.

Values of T_0 are shown in Table 1. For a specific polymer, comparable values of T_0 are found independently of the considered motion. This independence observed using AS is in agreement with the fact that no more motions are observed below this temperature. Only one value of T_0 for a polymer is thus used in further calculations: it corresponds to the average of the value for each motion.

Since $C_2^g = T_g - T_0$, a link between T_g and T_0 exists. This difference, primarily considered as universal, depends on the architecture of the polymer. Such a dependency is clearly observed using AS (Figure 2), and in fact a linear relationship is found with a reliability factor of 99.89% (eq 7). This equation takes into account all the polymers, every type of motion, and also all the cooling rates (all the data are available in Tables S-1 and S-2, Supporting Information):

$$T_0 = 1.05 T_{g(simulated)} - 77 \text{ K} \quad (7)$$

Such a relation was reported by Bartenev for different degrees of tacticity in the PMMA chain.[49] Similar relationships between T_0 and T_g can also be inferred from experimental data reported in the literature.[25,50,51]

Using AS, the physical meaning of T_0 is accurately described. Moreover, a relationship between this temperature and T_g is established. Analysis of the energetic terms intervening in the VFT and AG equations can now be carried out.

Table 1. Comparison of Simulated T_gs, Vogel Temperature, T_0, Effective Activation Energy, B, and Fragility Index, D, Stemming from Backbone Dynamics (bb) and the Coupling between the Side Chain and the Backbone (bb/sc), Carried Out at the Cooling Rate of 1.2×10^{12} K/min

		T_0 (K)		B (kJ mol^{-1})		D	
polymer	T_g (K)	bb	bb/sc	bb	bb/sc	bb	bb/sc
PE	285 ± 2	216		12.5		7.0	
PMA	380 ± 3	318	312	13.9	8.4	5.3	3.2
i-PMMA	415 ± 3	358	353	13	10.2	4.4	3.5
s-PMMA	483 ± 3	430	428	13.7	15.4	3.8	4.3
PS	449 ± 3	402	391	12.8	12.4	3.9	3.8
i-PαMS	472 ± 5	420	417	13.5	15	3.9	4.3
s-PαMS	550 ± 4	502	500	13.6	18.9	3.3	4.5

3.3. Study of the Effective Activation Energy *B*. Remarks have first to be made about the designation of B and thus on its intrinsic physical description. It is actually related to an activation energy at very high temperature where the Arrhenius behavior occurs. Ferry thus considered RB as an apparent activation energy where R is the gas constant.[52] For a sake of clarity, R will be omitted in the remaining of the text. For Solunov,[51] it is related to the activation energy per basic molecular specie (BMS); the apparent activation energy is equivalent to z^2B, where z is the size of a CRR, $z = T/(T - T_0)$. Average activation energy was also used by some authors.[28] The term of effective activation energy is employed in this text.[26] The reason for this choice lies in the fact that its behavior with respect to T_g yields some physical significance.

3.3.1. Backbone Dynamics. Backbone dynamics is inferred from the study of the $\vec{u}_{CH}$ motion (Figure 1). The resulting effective activation energy does not exhibit significant variation

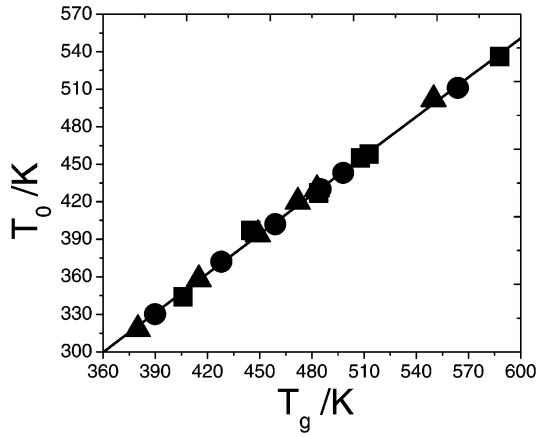

Figure 2. Average T_0s of studied polymers, reported with respect to simulated T_gs at three cooling rates: 1.2×10^{13} (■), 2.4×10^{12} (●), and 1.2×10^{12} K/min (▲). Linear fit (eq 7) is also displayed.

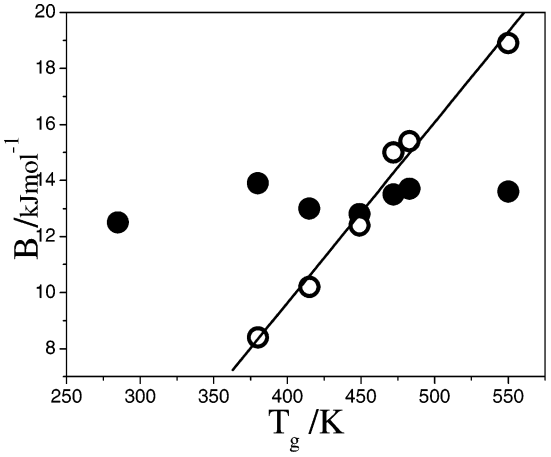

Figure 3. Effective activation energy, *B*, reported with respect to simulated T_gs at 1.2×10^{12} K/min cooling rate, for backbone dynamics (●) and backbone/side-chain coupling (○), for which the linear fit is also displayed.

with T_g, as is observed in Figure 3. A value of 13.4 ± 0.4 kJ/mol is obtained (Table 1). Since all polymers possess the same backbone, i.e., PE-like, *B* is directly linked to the intrinsic dynamics of the backbone. Moreover, its independence in relation to T_g indicates that all the polymer backbones exhibit the same behavior at a relative temperature above T_g. Experimentally, Bartenev et al. observed that relaxation processes in linear polymers containing the CH_2 group were characterized by a comparable effective activation energy, which was attributed to the backbone rotation. The physical significance of these results was understood according to the concept of free volume model.[53]

Similar behavior was observed using AS but with a different force field (*pcff*) for the two configurations of PMMA.[40] The difference between polymers dynamics at an absolute temperature thus comes from the presence of the side chain and its alternation. The dynamics resulting from the simultaneous consideration of motions described by bond vector $\vec{u}_{CO}$ or $\vec{u}_{CC}$ (Figure 1) is presented in the next section.

3.3.2. Backbone and Side-Chain Dynamics. As previously outlined, the behavior of the RACF of the vector associated with the side chain (Figure 1) with respect to time describes the coupling between the side chain and the backbone. Effective activation energy vs T_g is thus reported in Figure 3. Data are exposed in Table 1. A linear fit is revealed with a reliability factor of 99.19% (eq 8).

$$B = 0.064T_g - 16.15 \text{ kJ mol}^{-1} \quad (8)$$

Recently, a similar linear relationship between *B* and the experimental glass transition temperature of the *cis*-polyisoprene at different pressure was observed by Solunov.[54]

Several observations can be deduced from a linear relationship between *B* and T_g. Primarily, considering $B = 0$ in eq 8, a value of 254 K is obtained for the simulated T_g. This value has to be related with the simulated T_g of the amorphous linear PE, 285 K, at the same cooling rate (q_3). Such a comparison is worthwhile since the PE chain have only hydrogen atoms as their side chains. As a matter of fact, the adjunction of a side group to the main chain creates a perturbation that increases the T_g. It automatically yields a nonzero value for *B* due the coupling between the backbone and the side chain.

The dynamics which is characterized by the motion of the vector on the side chain includes several kinds of motions: mobility of the side chain, its rotation around the backbone, and motion of the backbone. This heterogeneity is at the origin of the observed variations in the value of T_g. Experimentally, using NMR relaxation, Spiess et al.[55] found that β-relaxation predominantly influences the time scale of the α-relaxation leading to a high mobility of the main chain itself. Using the multidimensional NMR, Schmidt-Rohr et al.[56] showed that the β process, relating to the side-chain rotation motion, is accompanied by a small backbone motion. Additionally, O'Reilly et al.[57] found that the difference in conformational energy of the backbone and side-chain motions in the PMMA decreases as the percentage of racemic diad increases. Vacatello and Flory[58] suggested that a greater exchange in energy between backbone and side-chain motions in the case of i-PMMA could explain this difference. This exchange was related to the cooperative motion between the side chain and backbone.[59] Consequently, the side-group rotation affects the thermal energy, effective activation energy, which is available to promote the coupling between the side group and the backbone. The same arguments are found using AS[60] and quasi-elastic neutron scattering[61] in the study of PMMA.

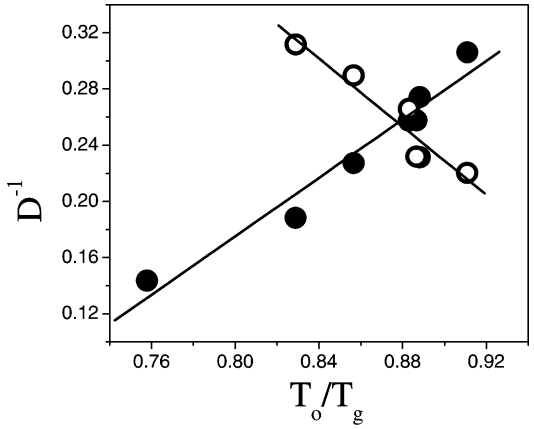

Figure 4. Fragility index, *D*, reported with respect to simulated T_0/T_g at 1.2×10^{12} K/min cooling rate, for backbone dynamics (●) and backbone/side-chain coupling (○); linear fits are also displayed.

Consequently, the general behavior of the two VFT fitting parameters stemming from AS is in agreement with experimental data. The behavior of the fragility index, i.e., the ratio of the two VFT entities *B* and T_0, can now be examined.

3.4. Behavior of the Fragility Index, *D*. Alike the effective activation energy *B*, the behavior of the fragility index *D* in relation to T_g is investigated. Dynamics associated with backbone motion and backbone/side-chain coupling are investigated. This strength parameter is directly linked to the fragility of supercooled liquids. Introduced by Angell,[62] the concept of fragility allows a classification scheme for such liquids. Rigid structures yield a low density of potential energy minima, which describes the energy landscape of strong liquids. Conversely, fragile liquids possess a great number of configurations, giving rise to a very high density of potential energy minima.

Values of *D* for both dynamics are shown in Table 1. The inverse of *D* is reported in Figure 4 with respect to T_0/T_g for both dynamics. Such a straight line reveals the fragility of the liquid as outlined by several authors.[1,46] In fact, the inverse of *D* is proportional to the fragility *m*.[45] A classification of polymers according to their fragility can thus be achieved. Considering only the backbone dynamics, PE is the strongest polymer, followed by PMA and i-PMMA (Table 1). s-PMMA, PS, and i-PαMS exhibit the same strength, while s-PαMS is the most fragile polymer. This fragility is in agreement with experimental data: PE < PMA < PMMA < PS where PS is

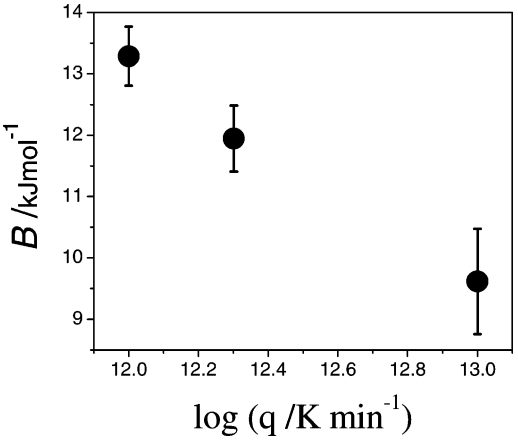

Figure 5. Effective activation energy, *B*, stemming from the study of the backbone dynamics, reported with respect of the logarithm of cooling rate.

the most fragile polymer.[63,64] The fact that PE backbone yields the highest *D* is thus not surprising: its simplified architecture gives rise to less potential wells. The same argument is valid for PMA with its more simplified side chain among the studied polymers.

A clearly different behavior is observed when the backbone/side-chain coupling is considered (Table 1 and Figure 4). In that case, PMA becomes the most fragile polymer and s-PαMS the strongest. As outlined by Dubowicz et al.,[28] the relative rigidity of the side chain affects the structural relaxation time which is disclosed by the AG equation. A higher fragility resulting from the coupling between the side chain and the backbone yields a lower fragility for backbone, and vice versa (Figure 4). The agreement between simulated and experimental data supports the use of AS in dealing with the glass transition phenomenon. A detailed analysis of the fragility from an atomistic simulation viewpoint was thus undertaken and will be the subject of an incoming article.

3.5. Influence of the Cooling Rate. The final section of this article concerns the incidence of the cooling rate on the values of *B* and *D*; it was shown that the ratio T_0/T_g is not affected by the cooling rate (Figure 2). Because of the lack of data, a detailed analysis cannot be carried out: all the data are available in Tables S-3 and S-4 in the Supporting Information. However, tendencies are outlined and reveal similar behavior: both *B* and *D* increase as the cooling rate decreases. As a representative example, the average value of the effective activation energy stemming from the study of backbone dynamics is reported with respect to the logarithm of the cooling rate, *q*, in Figure 5. As the cooling rate is decreased, a greater exploration of the phase space is achieved, and the resulting correlation time becomes longer. Such an increase in τ leads undoubtedly to an increase of both the effective activation energy and the fragility index.

4. Conclusion

Local dynamics of nine vinylic polymers were examined using atomistic simulation in order to extract parameters intervening in the VFT equation. According to the selection of appropriate bond vectors, two dynamics were revealed: backbone dynamics and coupling between the side chain and the backbone. The behavior of two VFT fitting parameters with respect to T_g were specifically studied: the Vogel temperature, T_0, and the effective activation energy, *B*. T_0 was thus found to be equal for either dynamics, in agreement with the fact that, by definition, no motions, save vibrations, occur under this temperature. Considering the dynamics associated with the backbone motion, the effective activation energy was found roughly constant, while it varies linearly with T_g when the dynamics resulting from the coupling between the side chain and the backbone is considered. A nonzero value for *B* was thus attributed to the coupling between the side chain and the backbone. The ratio of the two VFT entities, T_0 and *B*, yields the fragility index, *D*, occurring in the AG model. The inverse of *D* is actually proportional to the fragility. A direct comparison with experimental data was thus carried out. Data stemming from the consideration of backbone dynamics show good accuracy. However, values extracted from the backbone/side chain exhibit an opposite behavior, thus revealing the importance of coupling during the glass transition phenomenon. Such behaviors pave the way for a broader treatment of fragility,[65] using atomistic simulation.

Acknowledgment. The present work was supported by the Natural Sciences and Engineering Research Council (NSERC) of Canada and Université de Sherbrooke. Computations have been made possible thanks to the Canadian Fund Innovation (CFI), the Fonds Québécois de la Recherche sur la Nature et les Technologies (FQRNT), and Réseau Québécoise de Calcul Haute Performance (RQCHP). The authors thank R. Vadnais for the English corrections.

Supporting Information Available: Comparisons of simulated T_g (Table S-1), Vogel temperatures T_0 (Table S-2), effective activation energies *B* (Table S-3), and fragility indices *D* (Table S-4). This material is available free of charge via the Internet at http://pubs.acs.org.

References and Notes

(1) Donth, E. *The Glass Transition*; Springer-Verlag: New York, 2001.
(2) Ngai, K. L. *J. Non-Cryst. Solids* **2007**, *353*, 709−718.
(3) Robertson, R. E. Free-volume theory and its application to polymer relaxation in the glassy state. In *Computational Modeling of Polymers*; Bicerano, J., Ed.; Marcel Dekker: New York, 1992; pp 297−361.
(4) Gibbs, J. H.; Di Marzio, E. A. *J. Chem. Phys.* **1958**, *28*, 373−383.
(5) Adam, G.; Gibbs, J. H. *J. Chem. Phys.* **1965**, *43*, 139−146.
(6) Gotze, W.; Sjogren, L. *Rep. Prog. Phys.* **1992**, *55*, 241−376.
(7) Ngai, K. L. *Comments Solid State Phys.* **1979**, *9*, 127−140.
(8) Ngai, K. L. *Comments Solid State Phys.* **1980**, *9*, 141−155.
(9) Goldstein, M. *J. Chem. Phys.* **1969**, *51*, 3728−3739.
(10) Schulz, M. *Phys. Rev. B* **1998**, *57*, 11319−11333.
(11) Debenedetti, P. G.; Stillinger, F. H. *Nature (London)* **2001**, *410*, 259−267.
(12) Buhot, A.; Garrahan, J. P. *Phys. Rev. Lett.* **2002**, *88*, 225702.
(13) Garrahan, J. P.; Chandler, D. *Proc. Natl. Acad. Sci. U.S.A.* **2003**, *100*, 9710−9714.
(14) Gotze, W. *J. Phys.: Condens. Matter* **1999**, *11*, A1−A45.
(15) Ngai, K. L.; Capaccioli, S. *J. Phys.: Condens. Matter* **2007**, *19*, 250114.
(16) Berthier, L.; Biroli, G.; Bouchaud, J. P.; Cipelletti, L.; El Masri, D.; L'Hote, D.; Ladieu, F.; Pierno, M. *Science* **2005**, *310*, 1797−1800.
(17) Ediger, M. D. *Annu. Rev. Phys. Chem.* **2000**, *51*, 99−128.
(18) Glotzer, S. C.; Paul, W. *Annu. Rev. Mater. Res.* **2002**, *32*, 401−436.
(19) Colmenero, J.; Narros, A.; Alvarez, F.; Arbe, A.; Moreno, A. J. *J. Phys.: Condens. Matter* **2007**, *19*, 205127.
(20) van der Giessen, E.; Bulacu, M. *Phys. Rev. E* **2007**, *76*, 011807.
(21) Binder, K.; Baschnagel, J.; Paul, W. *Prog. Polym. Sci.* **2003**, *28*, 115−172.
(22) Bashnagel, J. *J. Phys.: Condens. Matter* **1996**, *8*, 9599−9603.
(23) Buchholz, J.; Paul, W.; Binder, K. *J. Chem. Phys.* **2002**, *117*, 7364−7372.
(24) Soldera, A.; Metatla, N. *Phys. Rev. E* **2006**, *74*, 061803.
(25) Cangialosi, D.; Alegria, A.; Colmenero, J. *Europhys. Lett.* **2005**, *70*, 614−620.
(26) Binder, K.; Baschnagel, J.; Paul, W. *Prog. Polym. Sci.* **2003**, *28*, 115−172.
(27) Debenedetti, P. G. *Metastable Liquids-Concepts and Principles*; Princeton University Press: Princeton, NJ, 1996.
(28) Dudowicz, J.; Freed, K. F.; Douglas, J. F. *J. Chem. Phys.* **2006**, *124*, 024906.

(29) Dudowicz, J.; Freed, K. F.; Douglas, J. F. *J. Phys. Chem. B* **2005**, *109*, 21350−21356.
(30) Karasz, F. E.; MacKnight, W. J. *Macromolecules* **1968**, *1*, 537−540.
(31) Metatla, N.; Soldera, A. *Mol. Simul.* **2006**, *32*, 1187−1193.
(32) Theodorou, D. N.; Suter, U. W. *Macromolecules* **1985**, *18*, 1467−1478.
(33) Roe, R. J. *J. Non-Cryst. Solids* **1998**, *235*−*237*, 308−313.
(34) Kovacs, A. J. *Adv. Polym. Sci.* **1964**, *3*, 394−508.
(35) Smith, W.; Forrester, T. R. *J. Mol. Graphics* **1996**, *14*, 136−141.
(36) Soldera, A.; Metatla, N. *Composites, Part A* **2005**, *36*, 521−530.
(37) Allen, M. P.; Tildesley, D. J. *Computer Simulation of Liquids;* Clarendon Press: Oxford, 1987.
(38) Berendsen, H. J. C.; Postma, J. P. M.; Van Gunsteren, W. F.; DiNola, A.; Haak, J. R. *J. Chem. Phys.* **1984**, *81*, 3684−3690.
(39) Soldera, A. *Macromol. Symp.* **1998**, *133*, 21−32.
(40) Soldera, A.; Grohens, Y. *Macromolecules* **2002**, *35*, 722−726.
(41) Kim, E. G.; Mattice, W. L. *J. Chem. Phys.* **1994**, *101*, 6242−6254.
(42) Antoniadis, S. J.; Samara, C. T.; Theodorou, D. N. *Macromolecules* **1998**, *31*, 7944−7952.
(43) Haile, J. M. *Molecular Dynamics Simulation*; John Wiley & Sons: New York, 1992.
(44) Lyulin, A. V.; Balabaev, N. K.; Michels, M. A. J. *Macromolecules* **2003**, *36*, 8574−8575.
(45) Böhmer, R.; Ngai, K. L.; Angell, C. A.; Plazek, D. J. *J. Chem. Phys.* **1993**, *99*, 4201−4209.
(46) Angell, C. A.; Borick, S. *J. Non-Cryst. Solids* **2002**, *307*−*310*, 393−406.
(47) Hodge, I. M. *J. Res. Natl. Inst. Stand.* **1997**, *102*, 195−205.
(48) Martinez, L. M.; Angell, C. A. *Nature (London)* **2001**, *410*, 663−667.
(49) Bartenev, G. M. *Vysokomol. Soedin., A* **1999**, *41*, 607−614.
(50) Angell, C. A. *J. Res. Natl. Inst. Stand.* **1997**, *102*, 171−185.
(51) Solunov, H. A. *J. Non-Cryst. Solids* **2006**, *352*, 4871−4876.
(52) Ferry, J. D. *Viscoelastic Properties of Polymers*, 2nd ed.; Wiley: New York, 1970; p 671.
(53) Bartenev, G. M.; Barteneva, A. G. *Vysokomol. Soedin., B* **1997**, *39*, 993−1000.
(54) Solunov, C. A. *J. Phys.: Condens. Matter* **2002**, *14*, 7297−7309.
(55) Kuebler, S. C.; Schaefer, D. J.; Boeffel, C.; Pawalzik, U.; Spiess, H. W. *Macromolecules* **1997**, *30*, 6597−6609.
(56) Schmidt-Rohr, K.; Kulik, A. S.; Beckham, H. W.; Ohlemacher, A.; Pawelzik, U.; Boeffel, C.; Spiess, H. W. *Macromolecules* **1994**, *27*, 4733−4745.
(57) O'Reilly, J. M.; Mosher, R. A. *Macromolecules* **1981**, *14*, 602−608.
(58) Vacatello, M.; Flory, P. J. *Macromolecules* **1986**, *19*, 405−415.
(59) Grohens, Y.; Prud'homme, R. E.; Schultz, J. *Macromolecules* **1998**, *31*, 2545−2548.
(60) Soldera, A.; Grohens, Y. *Polymer* **2004**, *45*, 1307−1311.
(61) Genix, A. C.; Arbe, A.; Alvarez, F.; Colmenero, J.; Farago, B.; Wischnewski, A.; Richter, D. *Macromolecules* **2006**, *39*, 6260−6272.
(62) Angell, C. A. *Science* **1995**, *267*, 1924−1935.
(63) Qin, Q.; McKenna, G. B. *J. Non-Cryst. Solids* **2006**, *352*, 2977−2985.
(64) Huang, D. H.; Colucci, D. M.; McKenna, G. B. *J. Chem. Phys.* **2002**, *116*, 3925−3934.
(65) Sokolov, A. P.; Novikov, V. N.; Ding, Y. *J. Phys.: Condens. Matter* **2007**, *19*, 205116.

MA071788+